

Article

Optimizing Renewable Injection in Integrated Natural Gas Pipeline Networks Using a Multi-Period Programming Approach

Emmanuel Ogbe^{1,2}, Ali Almansoori² , Michael Fowler¹  and Ali Elkamel^{1,2,*} 

¹ Department of Chemical Engineering, University of Waterloo, 200 University Avenue West, Waterloo, ON N2L 3G1, Canada

² Department of Chemical Engineering, Khalifa University of Science, Technology and Research (KUSTAR), Abu Dhabi P.O. Box 2533, United Arab Emirates

* Correspondence: aelkamel@uwaterloo.ca

Abstract: In this paper, we propose an optimization model that considers two pathways for injecting renewable content into natural gas pipeline networks. The pathways include (1) power-to-hydrogen or PtH, where off-peak electricity is converted to hydrogen via electrolysis, and (2) power-to-methane, or PtM, where carbon dioxide from different source locations is converted into renewable methane (also known as synthetic natural gas, SNG). The above pathways result in green hydrogen and methane, which can be injected into an existing natural gas pipeline network. Based on these pathways, a multi-period network optimization model that integrates the design and operation of hydrogen from PtH and renewable methane is proposed. The multi-period model is a mixed-integer non-linear programming (MINLP) model that determines (1) the optimal concentration of hydrogen and carbon dioxide in the natural gas pipelines, (2) the optimal location of PtH and carbon dioxide units, while minimizing the overall system cost. We show, using a case study in Ontario, the optimal network structure for injecting renewable hydrogen and methane within an integrated natural gas network system provides a \$12M cost reduction. The optimal concentration of hydrogen ranges from 0.2 vol % to a maximum limit of 15.1 vol % across the network, while reaching a 2.5 vol % at the distribution point. This is well below the maximum limit of 5 vol % specification. Furthermore, the optimizer realized a CO₂ concentration ranging from 0.2 vol % to 0.7 vol %. This is well below the target of 1% specified in the model. The study is essential to understanding the practical implication of hydrogen penetration in natural gas systems in terms of constraints on hydrogen concentration and network system costs.

Keywords: power-to-gas; methanation; multi-period optimization; pipeline optimization; renewable integration; mixed-integer non-linear programming (MINLP)



Citation: Ogbe, E.; Almansoori, A.; Fowler, M.; Elkamel, A. Optimizing Renewable Injection in Integrated Natural Gas Pipeline Networks Using a Multi-Period Programming Approach. *Energies* **2023**, *16*, 2631. <https://doi.org/10.3390/en16062631>

Academic Editor: Yukun Hu

Received: 30 December 2022

Revised: 15 February 2023

Accepted: 20 February 2023

Published: 10 March 2023



Copyright: © 2023 by the authors. Licensee MDPI, Basel, Switzerland. This article is an open access article distributed under the terms and conditions of the Creative Commons Attribution (CC BY) license (<https://creativecommons.org/licenses/by/4.0/>).

1. Introduction

The United State Energy Information and Administration or EIA reports that energy-related carbon dioxide or CO₂ emissions reached their highest record in 2021—this is after the decline in 2020 due to the pandemic [1,2]. The increase in CO₂ emission continues to pose a threat to consolidated efforts by society to mitigate the impact of climate change. The main source of CO₂ is from the combustion of fossil fuels. Natural gas remains the most clean, lowest cost energy option, especially for hard-to-electrify systems, compared to burning coal or petroleum products [3]. Reducing the content of CO₂ in natural gas is crucial to current efforts to mitigate climate change. In Canada, there are regulations that have been proposed for potentially increasing the renewable content in natural gas [4,5].

Despite technological strides in recent years concerning renewable energies, such as solar and wind, the cost of these technologies make them less competitive with traditional fossil fuels [3]. To bridge the gap between costly renewable energy options and traditional fossil fuels, natural gas provides a relatively low-emission fuel alternative to the more

expensive renewable fuel sources [6]. Furthermore, natural gas and the natural gas network has the ability to incorporate renewable content in the form of hydrogen blends via hydrogen injection or a mixture of synthetic natural gas, also known as synthetic methane or SNG from renewable sources, that can potentially help accelerate the development of renewable electricity [7]. However, with the current pipeline technology and end-use application, there are limits on the level of hydrogen that can be injected in the natural gas stream, otherwise known as hydrogen-enriched natural gas or HENG. The allowable limit is within a range of 5 to 20% [4,8] to avoid hydrogen permeating into the metal pipeline, otherwise known as hydrogen embrittlement.

Hydrogen is the key energy mix component in the quest for sustainability and reducing the CO₂ footprint of natural gas [8,9] as well as an essential transitional energy that can be efficiently stored. Two technological pathways for integrating renewable hydrogen and synthetic methane into natural gas pipelines are studied. These concepts benefit from the high storage capacity of the natural gas network or grid and do not require any modification of the current natural gas network. The concept generally requires a hydrogen intermediate; involving converting electrical energy directly into chemical energy in gaseous form. The technology is generally referred to as power-to-gas, or PtG [10,11]; specifically termed as power-to-hydrogen, or PtH, for the hydrogen end product or power-to-methane, or PtM, for the methane end product [12]. In power-to-hydrogen (i.e., PtH), surplus renewable energy or near zero-emissions nuclear power is converted into hydrogen gas through electrolysis. The obtained hydrogen can then be injected into the natural gas grid in the form of hydrogen-enriched natural gas. In doing so, the hydrogen can displace natural gas, reducing greenhouse gas emissions and the reliance on high-carbon fuels. In the power-to-methane (i.e., PtM) pathway, off-peak electricity and excess renewable power (e.g., wind power) is used to produce hydrogen via electrolysis, and then the hydrogen is combined with captured CO₂ from biogas streams or large CO₂ emitters (e.g., cement plants) [4]; see Figure 1 for a description of the methanation process. The CO₂ combines with hydrogen to form synthetic natural gas or SNG [12–14]. Power-to-gas technologies are very useful for compensating short-term fluctuations because of their ability to provide elevated storage capacity combined with high charge/discharge periods [12].

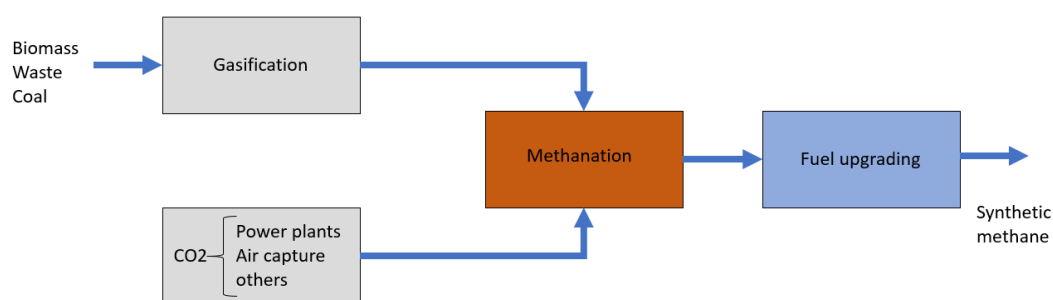


Figure 1. Methanation process.

The key argument to justify the immediate benefits for power-to-hydrogen is the fact that hydrogen can be seamlessly integrated into natural gas pipelines and delivered to end-users with minimum changes in infrastructure [10]. Transportation of natural gas from source, e.g., producing wells, etc., to destination, e.g., consumption regions, via natural gas pipelines has been extensively studied in the literature [6,15–17]. The pipeline system typically consists of a complex network that includes pipelines, compressor stations, regulators, valves, and city gates, among other components, that can be modelled using flow and pressure models.

In process systems engineering, steady-state operational models that contain multiple components typically involve the mixing or blending of different flow streams with different quality specifications. Examples include refinery optimization [18,19], multicomponent water networks [20,21], etc. To model the mixing of different flow streams of varied quality across the network, bilinear functions are typically used [18,22,23]. Similarly,

modelling the variation in natural gas quality after blending is important to accurately describe the behaviour of natural gas-blending systems [24,25]. Furthermore, modelling the pressure–flow relationship in natural gas systems is a necessary aspect of the model, but this introduces non-linearities that can further increase model complexity [26].

The systematic coupling of natural gas and power-to-gas hydrogen and methane can be motivated by a number of research works integrating natural gas with power transmission systems [27,28]. In a previous work, Ogbe et al. showed how hydrogen from power-to-gas can be integrated with a natural gas flow pipeline [29]. The authors used a pooling formulation to model hydrogen injection into a natural gas pipeline [26,30]. The work draws inspiration from numerous power-to-gas applications in the literature [11,31–33]. In this paper, in addition to integrating hydrogen and natural gas, another layer of decision making is included by the addition of a methanation unit to utilize the ever abundant CO₂ from different sources [12]. This second layer of modelling and decision making is required to further reduce carbon emission. Furthermore, we incorporate time varying behaviour into the design and operational problems using multi-period optimization. Multi-period optimization problems exist in natural gas models because certain parameters such as price of product, or the demand of gas production change from one season to another across the time horizon [15,34,35]. The multi-period integrated renewable injection in a natural gas pipeline is a mixed-integer non-linear program (MINLP) and takes the following form;

$$\begin{aligned} \min_{\substack{y \\ x_1, \dots, x_t}} \quad & \sum_{t=1}^{N_t} [f^0(y) + f_t^1(x_t)] \\ \text{s.t.} \quad & g^0(y) + g_t^1(x_t) \leq 0, \quad \forall t \in \{1, \dots, N_t\}, \\ & x_t \in X_t, \quad \forall t \in \{1, \dots, N_t\}, \\ & y \in \{0, 1\}^{n_y}, \end{aligned} \quad (1)$$

where $y \in \{0, 1\}^{n_y}$ are binary variables, while $x_t \in X_t, \forall t \in \{1, \dots, N_t\}$ are continuous variables. Typically all the functions $f^0 : \{0, 1\}^{n_y} \rightarrow \mathbb{R}$, $f_t^1 : X_t \rightarrow \mathbb{R}$, $g^0 : \{0, 1\}^{n_y} \rightarrow \mathbb{R}^m$, $g_t^1 : X_t \rightarrow \mathbb{R}^m$ are continuous and the set X_t is compact. Suppose an optimal solution for Problem (1) exist.

The main contributions of this paper are two-fold; firstly, we provide a novel mathematical modelling framework for integrating two hydrogen utilization pathways, using renewable hydrogen, synthetic methane and natural gas for a large-scale pipeline network system and secondly, we develop a multi-period model for the integrated system considering varying natural gas demand and electricity generation profiles. As far as the authors are aware, no other work has considered the systematic integration of methanation into natural gas pipelines in an optimization framework. We develop the integrated model as a series of sub-models constituting the overall problem; the first part consists of a power-to-hydrogen system, the second is a methanation system model where CO₂ and hydrogen are utilized for the production of synthetic methane, and the third is the integrated gas network system model. The details of these sub-models are presented in Section 4. A multi-period MINLP problem is consequently developed. The optimal solution of the optimization problem provides design and operational decisions across different time periods, providing valuable insights for the decision maker, leading to substantial savings in both investment and operating costs. The multi-period model employs the available electricity supply and natural gas demand data for the Ontario system by generating problem instances with an increasing number of time periods. This leads to a large-scale MINLP which is solved using ANTIGONE (algorithms for continuous/integer global optimization of non-linear equations) [36].

The remainder of the paper is organized as follows. In Section 2, a literature review of related work concerning integrated natural gas system design and operation will be presented, citing work on power-to-gas hydrogen blended with natural gas. Section 3 provides the generic framework used for process description and a general statement of the problem. Section 4 presents the multi-period integrated model for renewable (i.e., hydrogen

and synthetic methane) injections in a natural gas transportation system, from natural gas and hydrogen source locations to distribution centres, end-users or markets. Section 5 discusses the computational experiments for the integrated hydrogen and synthetic natural gas injection in natural gas pipelines. Section 6 presents the results and discussions and Section 7 presents the conclusions and suggestions for future work.

2. Related Literature

Injecting renewable hydrogen or methane into an integrated natural gas network is very closely related to existing work integrating natural gas into electricity networks. Unsihuay et al. developed an integrated model for natural gas-electricity networks in terms of optimal power and gas dispatch for the Belgium natural gas-electricity network [37]. Qui et al. developed a planning model for an integrated natural gas and power system network in Australia [38]. To model the integrated power and natural gas system, Correa-Posada and Sánchez-Martín posed a mixed-integer linear programming model that accounts for gas travelling velocity and compressibility [28]. Liu et al. developed a model for minimizing the coordinated social cost from a coupled electric power and natural gas transmission system [39]. El-Hadary et al. proposed a numerical model for the production of heat, electricity and hydrogen via a hydrogen electrolytic cell [40]. An optimal control model was developed by Chiang and Zavala to understand the systems dynamics in an interconnected natural gas and electricity transmission network [27]. More so, Calero et al. provided a review of energy storage systems in power grids [41].

One pathway for increasing renewable content in natural gas involves the injection of hydrogen generated from off-grid power sources. Garmsiri et al. studied the impact of hydrogen penetration from power-to-gas into a natural gas grid in southwestern Ontario [42]. Guandalini et al. studied the dynamic injection of hydrogen in the natural gas grid [43]. Eames et al. studied the impact of hydrogen blends (between 4.8 and 20%) and pipe geometry on mixing [44]. Su et al. developed a deep learning model to predict the mixing uniformity of hydrogen injection [45]. The impact of hydrogen fractions on pipeline natural gas quality was studied by multiple authors [46–48]. Integrating natural gas and hydrogen in pipeline transportation is very useful because of the number of high-value applications of hydrogen produced from power-to-gas, including vehicle or rail fuel (i.e., fuel cell vehicles), feedstock in industrial applications or hydrogen transportation to remote communities [43]. The introduction of hydrogen into the natural gas grid can potentially augment the natural gas in the form of ‘cleaner’ hydrogen-enriched natural gas. Ogbe et al. [29] extended the work conducted by previous authors concerning the problem of (1) injecting hydrogen across multiple pipelines and blending units, (2) modelling the bilinear non-linear characteristics associated with blending models, and (3) the impact of uncertainty in input parameters. They showed that the hydrogen concentration across multiple points can be strategically monitored and optimized. However, the study did not consider the temporal behaviour of the grid, in other words the periodic operation of an integrated system’s design and operation.

A second pathway involves the injection of both renewable hydrogen and synthetic methane in a natural gas pipeline system. Keogh et al. developed a grid simulation model that determines the annual grid capacity for synthetic/biomethane injection in Ireland [49]. The synthetic methane is generated by methanation utilizing CO₂ from different industrial units. In a methanation process, CO₂ is reacted with hydrogen in the Sabatier reactor to produce synthetic methane [12,14,50]. Different sources of CO₂ that produce substantial green house CO₂ emissions have been identified. The methanation pathway has the potential to consume a large amount of CO₂, significantly reducing the contribution to climate change. We are not aware of any work concerning a mathematical model that blends the methanation process with renewable hydrogen in a natural gas network.

Some literature have considered the use of mathematical programming approaches to understand the impact of renewable penetration in the form of hydrogen and SNG in natural gas networks. To model the design of natural gas pipeline networks integrated

with hydrogen injection, Wang et al. proposed mixed-integer linear programming (MILP) model. The authors reformulated the non-linearities in the pressure drop relationship using a piecewise linearization [51]. Jinpeng et al. proposed a two-stage stochastic mixed-integer non-linear programming (MINLP) framework for siting and sizing PtH, considering the system flexibility requirements. The authors used convex transformation techniques in order to reduce the computational burden [52]. Ogbe et al. proposed a MINLP model that determines the optimal concentration of hydrogen in a natural gas network. The authors used a global solver, BARON, to solve the optimization model [29].

In this paper, we propose two approaches for integrating hydrogen and synthetic methane into natural gas pipelines, while also considering the temporal impacts on the natural gas grid. The two approaches will be discussed in subsequent sections. Decision-making problems that consider the temporal behaviour can be modelled using multiple time periods, e.g., production rates, pressures, quantities of materials, etc., and are a function of time that leads to a multi-period programming formulation. The parameters in the model that vary over time include demand, supply, price, etc. [15,34,35]. Multi-period programming problems for the integrated natural gas network model leads to large-scale mixed-integer non-linear programs that generally require efficient algorithms to solve for global optimality [29,53] using a commercial solver. To the best of our knowledge, the method proposed in this paper is the only approach that explicitly considers intrinsic non-linearity associated with blending hydrogen and natural gas in an integrated system.

3. Process Description

We mathematically describe the renewable natural gas network problem as a graph, with units (e.g., an electrolyser) represented by nodes and connections represented by edges connecting nodes. The following notation is used to describe the system problem (see Figure 2). Let $s \in S$ represent the node in a set of sources, with nodes $e \in E$, $c \in C$ and $n \in N$ representing nodes belonging to the subset of sources for electrolyser (or hydrogen) units, CO₂ and natural gas, respectively, i.e., $E \cup C \cup N \subset S$. Furthermore, we denote the nodes in the blending units as $m \in M$ and demand nodes as $d \in D$. At the blending units, we assume ideal mixing [22], where natural gas streams with different components $k \in K$ are mixed or blended. Planning is carried out over a set time period $t \in \{1, \dots, H\} = T$, where H is the time horizon. Flows across nodes are characterized by symbols f in mol/day, e.g., the flow leaving source s and arriving at mixer m for a given time period $t \in T$ is given by $f_{n,m,t}$. For each natural gas source $n \in N$, the set of connecting blending units is given by $(n, m) \in \Theta_m$ and the set of connecting distribution centres is given by $(n, d) \in \Theta_d$. Similarly, for each hydrogen station, the set of blending units is denoted by $(e, m) \in \Pi_m$; while the set of connecting blending units to a carbon source is given by $(c, m) \in \chi_m$. Finally, for each blending unit, the set of connecting blending unit is denoted by $(m, m') \in \Lambda_{m'}$, while the set of connecting distribution centres is given by $(m, d) \in \Lambda_d$. The symbols \bigcirc and \square represent the sources and blending nodes, respectively, while forward pointing arrows \rightarrow denote the edges or pipeline connections between the nodes, and \triangle represents compression stations.

The multi-period problem for the integrated design and operation of renewable injections addressed in this work is an extension of the model in [29]. In [29], the problem of injecting hydrogen into natural gas pipelines was addressed by combining a power-to-hydrogen model and a natural gas model. The article also addressed the effect of uncertainty in natural gas demand and quality, and the optimal infrastructure and operational decisions across different uncertainty scenario. The model in this paper considers both the injection of hydrogen, as well as the injection of renewable methane (also called synthetic natural gas) into a natural gas network. The addition of a methanation model is particularly important because substantial levels of available CO₂ from processing plants needed for methanation can be curtailed by this methodology. We propose two conceptual superstructures for the integrated design and operation of (1) synthetic natural gas, or SNG, injection, and (2) the injection of both hydrogen and SNG, into a natural gas stream. Figure 3 describes the proposed conceptual design. Here, the renewable hydrogen-rich

stream is combined with a CO₂-rich stream. The output SNG stream is combined with the conventional gas stream in a natural gas pipeline network. In the second concept, hydrogen is reinjected at the mixing point, i.e., θ in Figure 3 is different from one. The overall model combines the following sub-models; (1) power-to-hydrogen (PtH) model, (2) methanation model, and (3) natural gas flow and pressure model, bridging the constraints linking the different sub-models. More information on the two designs is provided in Section 6. Figure 2 describes the detailed network interconnections between nodes for hydrogen, SNG and natural gas units. Furthermore, the time variation of parameters, such as electricity supply and natural gas demand across time, are included in the model so as to obtain the most economic design over the time horizon. The PtH model entails the conversion of renewable electricity to hydrogen across different units E1, E2, ... via electrolysis. In the methanation model, CO₂ from different sources, C1, C2, ... (e.g., power plants, steel plants, biogas units, etc. [12,54,55]) are combined with hydrogen from the PtH model in reactors R to produce SNG for onward injection into the third system, i.e., the integrated gas system. The natural gas system consists of potential natural gas sources labelled N1, N2, ... to be developed, blending units labelled M1, M2, ... and distribution stations D1, D2, ... across the network.

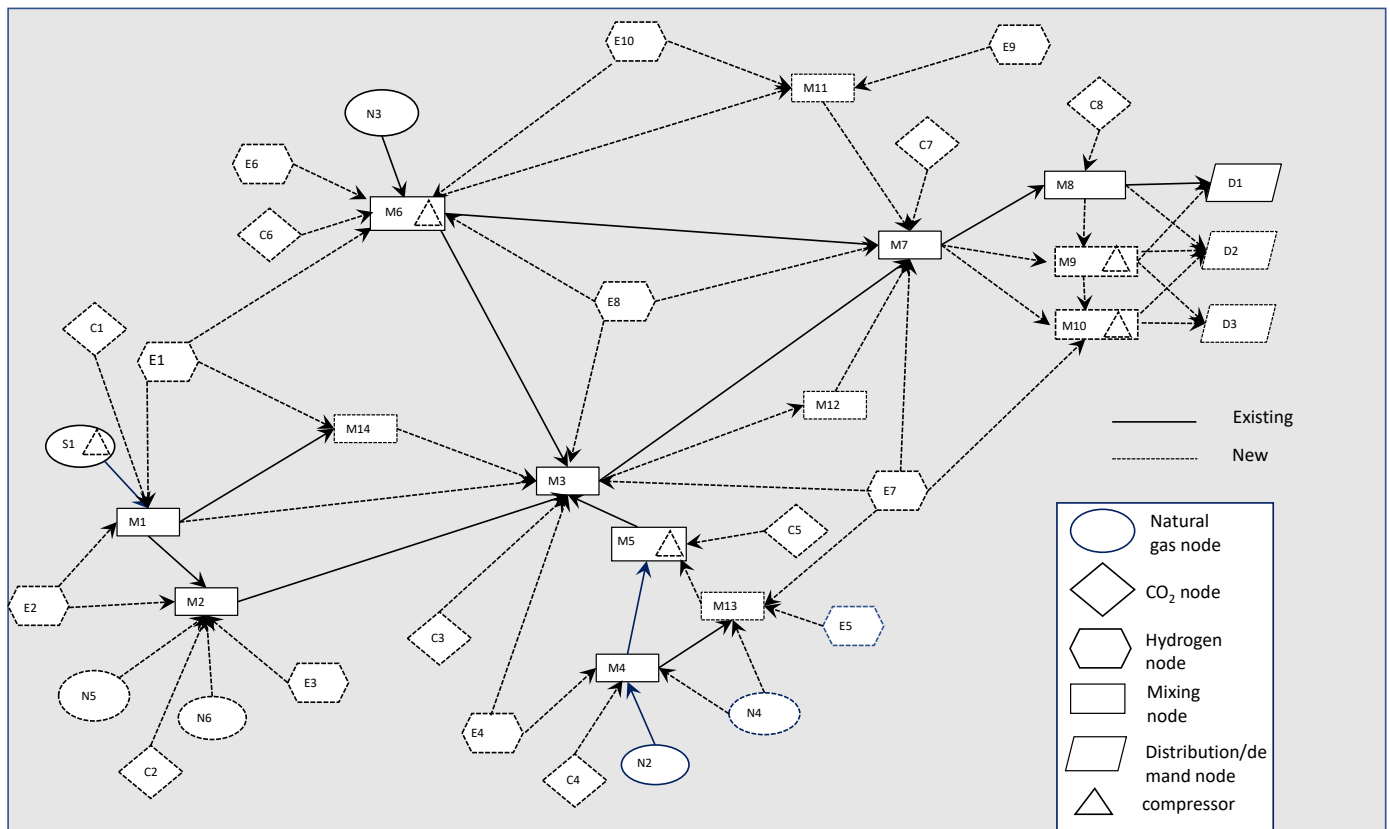


Figure 2. Superstructure for renewable injection in the Ontario natural gas grid (pipeline distance not to scale).

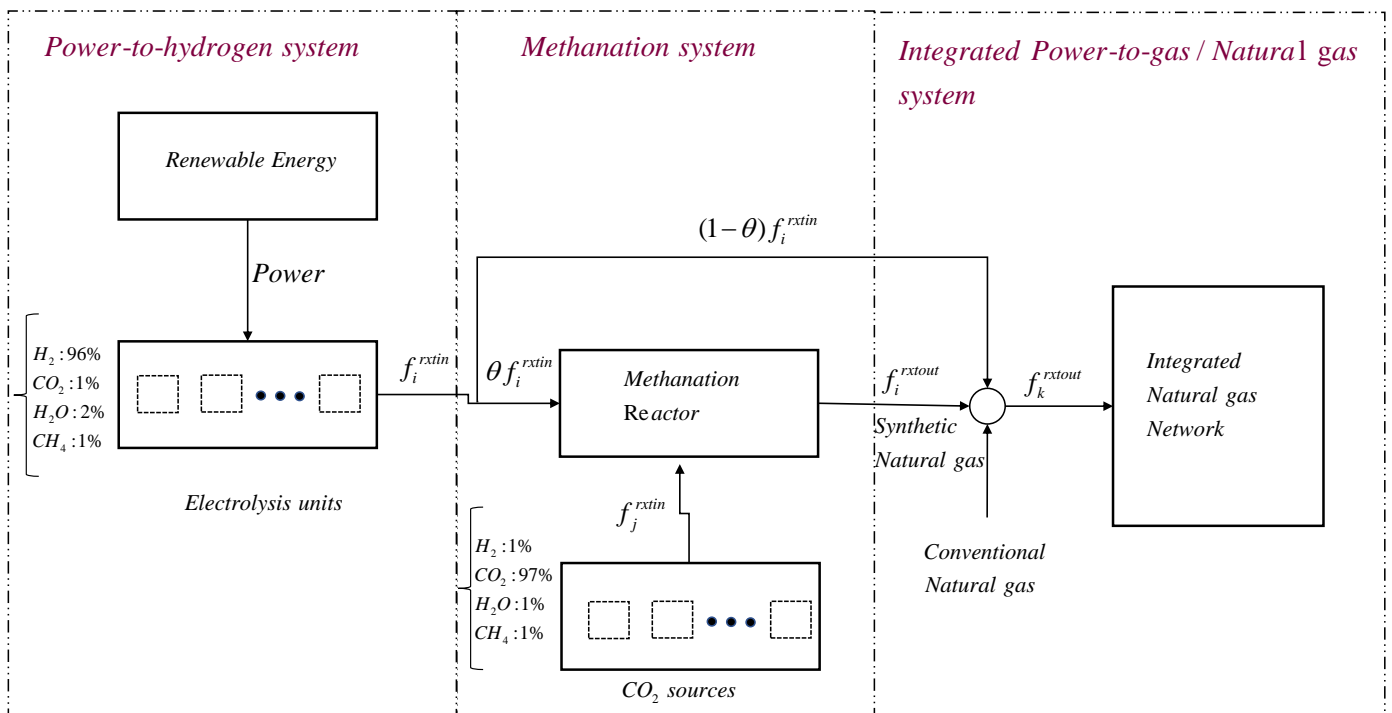


Figure 3. Process description for combined methanation and hydrogen injections.

The integrated system model optimizes both the design and operational decisions. Binary decision variables are used to model design decisions which include whether or not to include electrolyser/hydrogen stations, CO₂ sources, natural gas sources, blending or distribution units and connections between them, while continuous variables model the operational variables consisting of flow rates and pressures at the different nodal locations and at the units/pipeline connections. The binary variables given by y_e, y_c, y_n, y_m and y_d denote the nodes for electrolysis, CO₂, natural gas, blending and distribution units, respectively, while $y_{e,r}, y_{c,r}, y_{r,m}, y_{n,m}, y_{n,d}, y_{m,m'},$ and $y_{m,m'}$ denote the design connections between the different sources to blending, and blending points to distribution centres. The flow rates over a given time period $t \in T$, with different qualities $w \in W$ after blending, are given by $f_{e,r,t}, f_{c,r,t}, f_{r,m,t}, f_{n,m,t}, f_{n,d,t}, f_{m,m',w,t}$ and $f_{m,d,w,t}$ which denotes pipeline flows from sources to blenders, flows between blenders, and blenders to distribution units. To reduce complexity, the model only includes pressure variables for the upstream pressures at a natural source, hydrogen unit, blender or distribution centres, $p_{n,t}^{ups}, p_{m,t}^{ups}, p_{d,t}^{ups}$ and $p_{n,t}^{dws}, p_{m,t}^{dws}, p_{d,t}^{dws}$ for downstream pressure at a natural gas source, hydrogen unit, blender and distribution centres, respectively. See Figure 3 for a process description of the methanation process. Note that we use bold fonts to distinguish between variables and parameters, see nomenclature section.

The multi-period optimization of an integrated design and operation problem for hydrogen and SNG injection in natural gas networks is stated as follows:

Maximize the profitability of an integrated hydrogen–CO₂–natural gas network system, while satisfying the hydrogen and CO₂ concentration requirements and other product-specific constraints for all time periods across the time horizon.

The optimization requires the following data to be available:

1. An available or conceptual superstructure for the hydrogen–methanation–natural gas-integrated network;
2. Surplus electricity generation profiles at the different hydrogen production nodes and at different time periods $\forall t \in T$;
3. Sources of CO₂ and natural gas and their available capacity at different time periods $\forall t \in T$;

4. Demand profiles for hydrogen and natural gas across different time periods $\forall t \in T$;
5. Data on the capacities of the sources, blending units, distribution centres and pipelines;
6. Cost associated with the sources, blenders or blending units, and distribution centres and their interconnecting pipelines.

4. Mathematical Modelling of an Integrated System for Renewable Injections

4.1. Power-to-Hydrogen Model

For the typical kind of electrolyser (the PEM electrolyser), authors in [56,57] predicted the rate of hydrogen production from electrolysis as proportional to power consumption. A time-based formulation where we specify the hydrogen production for every time period is given by Equations (2)–(4);

$$f_{e,m,t} = \eta E_{e,t} HHV, \tag{2}$$

$$y_e \times E^{lo} \leq E_{e,t} \leq y_e \times E^{up}, \tag{3}$$

$$E_{e,t} \leq E_e^{surpl}, \tag{4}$$

$$\forall e \in E, \forall r \in R, \forall m \in M, \forall t \in T.$$

Equation (2) denotes the conversion of electrical energy to hydrogen in the hydrogen production system, where η is the efficiency. Equation (3) specifies the bounds on electricity generation. The PEM electrolyser module chosen in this study has a unit size of 1000 kW [58], with 10 electrolysers installed for a given node e , i.e., the upper bound on a single electrolyser module, $E^{up} = 10 \times 1000$ kW-day. The lower bound in Equation (3) denotes the lowest level at which the electrolysers can operate, and E^{lo} is set at zero kW-day for this work. The amount of surplus baseload electricity for each node e available is denoted by the parameter E_e^{surpl} (kW-day). In Equation (3), y_e is a binary variable that determines the power-to-gas node in the network. Equation (4) specifies that the total energy required by the electrolysers must be less than or equal to the surplus electricity.

4.2. Methanation Model

The model for the conversion of CO₂ to SNG consists of the following; a total mass balance and a component balance with a reaction conversion term. Note that for convenience, we assume that a 100% capacity at the CO₂ sources can be transmitted to the reactor, i.e., $y_c = y_{cr}$. The methanation model is as follows:

$$\sum_{e \in E} f_{e,r,t}^{H_2,rxin} + \sum_{c \in C} f_{c,r,t}^{CO_2,rxin} = \sum_{m \in M} f_{r,m,t}^{rxout} \tag{5}$$

$$p_1 \sum_{e \in E} f_{e,r,t}^{H_2,rxin} + p_2 \sum_{c \in C} f_{c,r,t}^{CO_2,rxin} - conv \left(p_1 \sum_{e \in E} f_{e,t}^{H_2,rxin} + p_2 \sum_{c \in C} f_{c,t}^{CO_2,rxin} \right) = p_3 \sum_{m \in M} f_{r,m,t}^{rxout} \tag{6}$$

$$f_{e,r,t}^{H_2,rxin} \leq y_e F_{e,t}^{H_2,up} \tag{7}$$

$$f_{c,r,t}^{CO_2,rxin} \leq y_c F_{c,t}^{CO_2,up} \tag{8}$$

$$f_{m,r,t}^{rxout} \leq y_m F_{m,t}^{up} \tag{9}$$

$$\forall e \in E, \forall c \in C, \forall m \in M, \forall r \in R, \forall t \in T.$$

Equation (5) describes the total mass balance around the reactor indexed r , with hydrogen node e and CO₂ inlet stream indexed c . Equation (6) is the component balance in the steady state, with the conversion term denoting the reaction extent; p_1 , p_2 and p_3 represent the mole fraction of components in the stream while $conv$ is the conversion limit. Equations (7)–(9) limit the hydrogen, CO₂ and reactor products within some upper bound.

4.3. Integrated Gas Distribution Model Flow Model

The flow model presents the relationships between flow rates at the different nodes and interconnections within the pipeline network. The design decisions on sources, mixers, end users and connections between them, are denoted by the $y_n, y_{m'}, y_d, y_{n,m'}, y_{n,d}$ and $y_{m,d}$ binary variables. The subscripts associated with a variable denote the individual node elements or connections between nodes. The operational decisions for every period $t \in T$ are represented by $f_{n,m,t}, f_{n,d,t}, f_{m,d,w,t}$ and $f_{m,m',w,t}$ and the maximum allowed capacities for the flow rates are denoted by $F_{n,m}^{up}, F_{n,d}^{up}, F_{m,d}^{up}$ and $F_{m,m'}^{up}$. A comprehensive list of all sets, variables and parameters is given in Nomenclature. All design and operational decision variables described in this paper are non-negative. The model for the sources, blending units and end users is given below.

$$y_{n,m} F_{n,m}^{lo} \leq f_{n,m,t} \leq y_{n,m} F_{n,m}^{up} \tag{10}$$

$$y_{n,d} F_{n,d}^{lo} \leq f_{n,d,t} \leq y_{n,d} F_{n,d}^{up} \tag{11}$$

$$y_{e,m} F_{e,m}^{lo} \leq f_{e,m,t} \leq y_{e,m} F_{e,m}^{up} \tag{12}$$

$$y_{m,m'} F_{m,m'}^{lo} \leq \sum_{k \in K} f_{m,m',k,t} \leq y_{m,m'} F_{m,m'}^{up} \tag{13}$$

$$y_{m,d} F_{m,d}^{lo} \leq \sum_{k \in K} f_{m,d,k,t} \leq y_{m,d} F_{m,d}^{up} \tag{14}$$

$$\left(\sum_{m \in \Pi_m} \sum_{k \in K} f_{m,d,k,t} + \sum_{n \in \Theta_d} f_{n,d,t} \right) V_{d,k}^{lo} \leq \sum_{m \in \Pi_d} f_{m,d,k,t} + \sum_{n \in \Theta_{n,d}} f_{n,d,t} U_{n,k} \tag{15}$$

$$\sum_{m \in \Pi_m} f_{m,d,k,t} + \sum_{n \in \Theta_d} f_{n,d,t} U_{n,k} \leq \left(\sum_{m \in \Pi_d} \sum_{k \in K} f_{m,d,k,t} + \sum_{n \in \Theta_d} f_{n,d,t} \right) V_{d,k}^{up} \tag{16}$$

$$H_2 frac_{m,d,t} \leq \left(f_{m,d,t}^{H_2} / \sum_{k \in K} f_{m,d,k,t} \right) V_d^{H_2,up} \tag{17}$$

$$CO_2 frac_{m,d,t} \leq \left(f_{m,d,t}^{CO_2} / \sum_{k \in K} f_{m,d,k,t} \right) V_d^{CO_2,up} \tag{18}$$

$$y_d Dem_{d,t}^{lo} \leq \sum_{m \in \Pi_{m,d}} \sum_{k \in K} f_{m,d,k,t} + \sum_{n \in \Theta_n} f_{n,d,t} \leq y_d Dem_{d,t}^{up} \tag{19}$$

$$y_{n,m} \geq y_{m'} \quad \forall n \in N, m \in M, \tag{20}$$

$$\forall n \in \Theta_m, \forall n \in \Theta_d, \forall e \in \Pi_m, \forall c \in \chi_m, \forall m \in \Lambda_{m'},$$

$$\forall d \in D, \forall k \in K, t \in T.$$

Capacity limits of all flows going out of the sources to different blending units and distribution points are given by Equation (10). On the other hand, Equations (11)–(14) require that flow from both the natural gas and the hydrogen sources to their respective destinations must respect the upper bounds. Equations (15) and (16) specify the capacity constraints for the blending units. They require that the total capacity of all pipelines connecting to a blending unit should be no less than the capacity of that blending unit.

Equations (17) and (18) require that the quality of hydrogen and CO₂ are within the set lower and upper limits. Additionally, Equations (17) and (18) constrain the concentration of hydrogen and CO₂ at the exit to be no more than an average set by the user, in % by volume at the exit site. Meanwhile, Equation (19) requires that the maximum and minimum demands at the distribution stations cannot be more than the total flows in the system, while Equation (20) enforces topological constraints that require that a source n is developed only if the links between source n and blending units m are developed.

4.4. Bridging Constraints

The following constraints provide the linkage between the three sub-models; hydrogen, methanation and natural gas models, in the integrated system. Equations (21) and (22) represent constraints for the material balance for the hydrogen–natural gas system, where s is the split fraction representing the fraction of flow to either the blending units or the distribution centres. They are used to control the amount of hydrogen and natural gas that is injected into the natural gas pipeline network. The constraints in Equations (21) and (22) require that the total hydrogen, SNG, and natural gas flow into a blending unit and distribution station be conserved. Equation (23) requires that the total split fraction sums to unity. Equation (24) constraints the total capacity of the hydrogen, CO₂ and natural gas to be within some upper bound. Equation (25) specifies that the flow of hydrogen to the methanation reactor unit is proportional to the flow from the electrolysis unit, while Equation (26) specifies that the flow of hydrogen to the natural gas network is no greater than the gas from electrolysis. θ_e is a variable denoting the fraction of flow split between methanation and the direct injection of hydrogen into the natural gas pipeline network.

$$f_{m,m',k,t} = s_{m,m',t} \left(\sum_{n \in \Theta_m} f_{n,m,t} U_{n,k} + \sum_{e \in \Pi_m} f_{e,m,t} V_{e,k} + \sum_{r \in R} f_{r,m,t}^{rxout} + \sum_{m \in \Pi_{m,m'}} f_{m,m',k,t} \right), \quad (21)$$

$$f_{m,d,k,t} = s_{m,d,t} \left(\sum_{n \in \Theta_m} f_{n,m,t} U_{n,k} + \sum_{e \in \Pi_m} f_{e,m,t} V_{e,k} + \sum_{r \in R} f_{r,m,t}^{rxout} + \sum_{m \in \Pi_{m,m'}} f_{m,m',k,t} \right), \quad (22)$$

$$\sum_{m \in \Lambda_{m'}} s_{m,m',t} + \sum_{d \in \Pi_{m,d}} s_{m,d,t} = 1, \quad s_{m,m',t}, s_{m,d,t} \geq 0, \quad (23)$$

$$\sum_{m \in M} f_{n,m,t} + \sum_{m \in M} f_{e,m,t} + \sum_{d \in D} f_{s,d,t} \leq y_n Z_{n,t}^{up} + y_e Z_{e,t}^{up}, \quad (24)$$

$$f_{e,t}^{rxin} \leq \theta_e f_{e,t}^{H_2}, \quad (25)$$

$$f_{e,m,t} \leq (1 - \theta_e) f_{e,t}^{H_2}, \quad (26)$$

$$\forall e \in E, \forall m \in M, \forall k \in K, \forall t \in T.$$

Note that the products of $s_{m,m',t}$ and $f_{n,m,t}$ in Equations (21) and (22) lead to bilinear terms.

4.5. Pressure Model

There is a pressure differential across each pipeline segment and the flow through the pipeline is assumed to follow the ideal gas relationship. We derive the pressure model based on the work of the authors in [26,29,59]:

$$y_{n,m} \left[(P_{n,t}^{ups})^2 - (P_{m,t}^{dws})^2 \right] = \kappa_{n,m} (f_{n,m,t})^2, \forall (n, m) \in \Theta_m, \forall t \in T \quad (27)$$

$$y_{e,m} \left[(P_{e,t}^{ups})^2 - (P_{e,t}^{dws})^2 \right] = \kappa_{e,m} (f_{e,m,t})^2, \forall (e, m) \in \Pi_m, \forall t \in T \quad (28)$$

$$y_{n,d} \left[(P_{n,t}^{ups})^2 - (P_{d,t}^{dws})^2 \right] = \kappa_{n,d} (f_{n,d,t})^2, \forall (n, d) \in \Theta_d, \forall t \in T, \quad (29)$$

$$P_{n,t}^{ups} - P_{n,t}^{dws} = 0, \forall n \in N, t \in T \quad (30)$$

$$P_{e,t}^{ups} - P_{e,t}^{dws} = 0, \forall e \in E, t \in T \quad (31)$$

$$P_{m,t}^{ups} - P_{m,t}^{dws} = 0, \forall m \in M, t \in T \quad (32)$$

$$P_{d,t}^{ups} - P_{d,t}^{dws} = 0, \forall d \in D, t \in T, \quad (33)$$

$$W_{i,t} - \alpha_i \sum_{j \in \{j:(i,j) \in N_{i,j}\}} f_{i,j,t} \left[\left(\frac{P_{i,t}^{dws}}{P_{i,t}^{ups}} \right)^v - 1 \right] = 0, \forall i \in C, t \in T, \quad (34)$$

$$y_i W_{i,t}^{lo} \leq W_{i,t} \leq y_i W_{i,t}^{up}, \forall i \in C, t \in T, \tag{35}$$

$$P_{n,t}^{ups} \geq P_{n,t}^{dws}, \forall n \in N, t \in T, \tag{36}$$

$$P_{n,t}^{downs} \geq P_{n,t}^{ups}, \forall n \in N, t \in T, \tag{37}$$

$$y_n P_n^{ups,lo} \leq P_{n,t}^{ups} \leq y_n P_n^{ups,up}, \forall n \in N, t \in T, \tag{38}$$

$$y_n P_n^{dws,lo} \leq P_{n,t}^{dws} \leq y_n P_n^{dws,up}, \forall n \in N, t \in T. \tag{39}$$

where $f_{n,m,t}$, $f_{e,m,t}$ and $f_{n,d,t}$ are the gas flow rates in the, respectively, pipelines; $\kappa_{n,m}$, $\kappa_{e,m}$, $\kappa_{n,d}$ and α_i are estimated coefficients based on the particular pressure–flow profile considered in the model, and $W_{i,t}$ is the power consumption. We adopt the values presented in Selot et al. [26].

Equations (27)–(29) represents the pressure–flow relationship for the pipelines from the natural gas source to mixing stations, hydrogen sources to mixing stations or mixing stations to distribution centres, respectively, while Equations (30)–(33) restricts the upstream and downstream pressure to be the same in the node. Equation (34) gives the power consumption equation for a gas compressor. The power is the sum total of the power output of all the compressors available in the facility. The bounds on power consumption for a given compressor is given by Equation (35). Equations (36) and (37) require that the upstream and downstream pressures are the same for connections between nodes. Equations (38) and (39) impose lower and upper bounds on the upstream and downstream pressures, respectively.

4.6. Objective Function

The objective function aims to maximize the annualized net present value (revenue) over a long-term planning horizon. The total revenue consist of (i) capital costs for transporting renewable hydrogen, methane and conventional natural gas, (ii) operating costs for transporting these different components, (iii) income generated from the sale of the natural gas/hydrogen blend and (iv) the power consumption of the compressors installed.

The objective function is given by the following, Equation (40):

$$Objective = Capcost + \sum_{t \in \{1, \dots, H\}} \frac{1}{(1+r)^t} (Opcost_t - Income_t), \tag{40}$$

where H is the time horizon [60]. The capital and operating costs for integrated hydrogen, methanation and natural gas are given by Equations (41) and (42), respectively, while the income is given by Equation (43). The term $\left(\frac{1}{(1+r)^t}\right)$ is used to discount the profits over the duration of the study, where r is the discount rate, t is the time index and T is the overall time period.

$$Capcost = \sum_{n \in N} c_n^{inv} y_n + \sum_{e \in E} c_e^{inv} y_e + \sum_{m \in M} c_m^{inv} y_m + \sum_{d \in D} c_d^{inv} y_d \tag{41}$$

$$Opcost_t = \left(\sum_{m \in \Theta_e} \sum_{e \in E} c_e^{op} f_{e,m,t} + \sum_{m \in \Theta_m} \sum_{d \in D} c_{m,d}^{op} f_{m,d,t} + \sum_{n \in N} \sum_{d \in D} c_{n,d}^{op} f_{n,d,t} \right) + \sum_{n \in N} c_n^{elec} W_{n,t} \tag{42}$$

$$Income_t = \sum_{d \in D} c_d^{pr} \left(\sum_{s \in \Pi_d} \sum_{w \in \Omega} f_{m,d,w,t} + \sum_{n \in \Theta_d} f_{n,d,t} \right) \tag{43}$$

where c_n^{inv} , c_e^{inv} , c_m^{inv} and c_d^{inv} are the investment costs associated with building the hydrogen and natural gas infrastructure; $c_{n,m}^{inv}$, $c_{e,m}^{inv}$, $c_{s,d}^{inv}$ and $c_{m,d}^{inv}$ are the investment costs for pipelines connecting the infrastructure units; c_n^{op} , c_e^{op} , $c_{m,d}^{op}$, $c_{n,d}^{op}$ are the operating costs; c_n^{elec} is the

electricity cost for running compression stations; and c_d^{pr} is the price of gas sold at the distribution station.

The multi-period programming model for the integrated model can be posed as the following:

minimize objective (Equation (40))
 s.t. Integrated hydrogen, methanation and natural gas model
 given by Equations (2)–(4), (5)–(9), (10)–(20), (21)–(26), (27)–(39), (41)–(43),
 $y_n, y_c, y_e, y_m, y_d, y_{n,m}, y_{e,m}, y_{c,m}, y_{n,d}, y_{m,m}$, and $y_{m,d}$ are binary,
 All flow rates and pressures are non-negative.

Notice that the above optimization problem is in the form of Problem (1), and it is therefore a mixed-integer non-linear (non-convex) programming problem (MINLP).

5. Computation Study

5.1. Tools/Implementation

The optimization model is a mixed-integer non-linear programming problem (MINLP) and is programmed using the General Algebraic Modeling Systems or GAMS ver 24.8.5 optimization platform [61]. The global optimization solver called ANTIGONE [36] is utilized to generate the optimal solution. CONOPT [62] and CPLEX [63] are used as the (local) non-linear and linear programming solvers, respectively. The optimization tolerance was set at 1%.

5.2. Case Study Problem Superstructure

We consider two approaches or problem settings in the design and operation of integrated system comprised of hydrogen, SNG and natural gas. In the first scenario denoted as Case A—shown in Figure 4, we consider the integration of SNG from methanation in a natural gas network. Case B considers the combined integration of a hydrogen, methanation and natural gas network system, and investigates the trade-offs between hydrogen injection, methanation or both. A third scenario is the case where hydrogen alone is integrated with natural gas in natural gas pipelines, presented in our earlier work [29] and so we do not consider that scenario in this paper. This model is otherwise known as the single-period optimization model. More details on the two cases will be provided in the next section. In the case study we consider, there are ten hydrogen stations, i.e., E1, ..., E10, and eight CO₂ sources, i.e., C1, C2, ..., C8 going into a reactor R. There are six potential natural gas sources labelled N1, N2, ..., N6 to be developed, fourteen blending units labelled M1, M2, ..., M14, and three distribution stations D1, ..., D3, across the network. The linking constraints connecting the three sub-models presented in Section 4, can sometimes be infeasible depending on the parameter settings. We avoid this problem by penalizing the violation of infeasible constraints using a penalty term, described by the authors in [64,65]. We provide a detailed feasibility problem formulation in the Appendix A. The optimal design and operation decisions for Case A, B are discussed in the proceeding subsection.

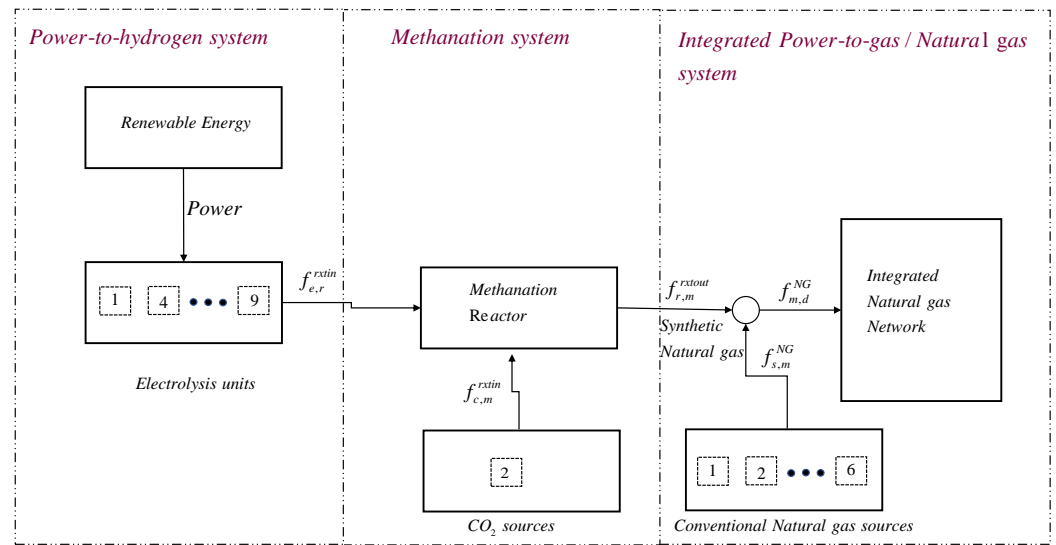


Figure 4. Process description for methanation in natural gas networks (Case A).

In the multi-period model for the integrated system, the demand of natural gas and electricity generation fluctuate with time. For this study, we collected daily data for the different zones in Ontario for one year. The partitioning of the planning horizon into time intervals is performed according to Figure 5, based on the strategy in [15], for the natural gas and excess electricity data for one year. The data for the study is based on Ontario data presented in our earlier work [29]. We consider a one year planning horizon and formulate different problem instances denoted by cases 1P, 2P, 6P, 12P, 18P and 24P depending on the time intervals or periods:

- 1P contains one time period only; equivalent to averaging the data over the entire year.
- 2P contains two time periods; equivalent to averaging data over a 6 month period.
- 6P contains 6 time periods; equivalent to averaging over a 2 month period.
- 12P contains 12 time periods; equivalent to averaging over an interval of one month.
- 18P contains 18 time periods; equivalent to averaging data over 3 weeks.
- 24P contains 24 time periods; equivalent to averaging over 2 weeks.

Period length / interval

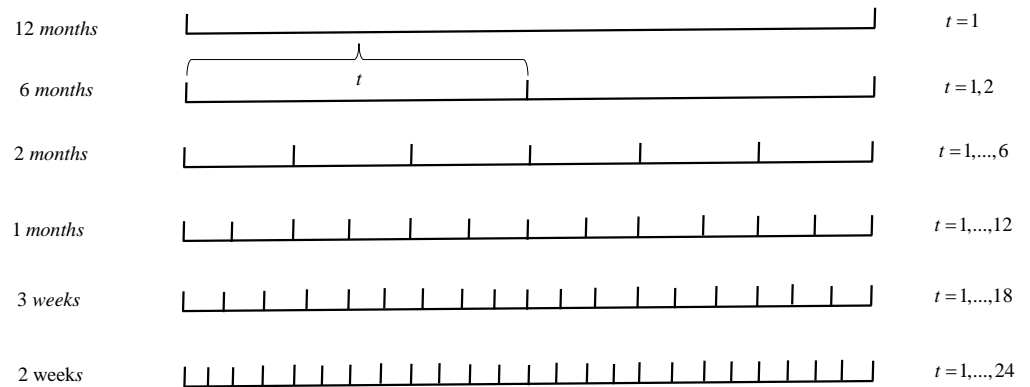


Figure 5. Number of time periods for the different multi-period problems.

6. Results and Discussion

We present the computational experiments for the integrated network model for the injection of renewables into natural gas pipelines using two case models; a single-period model and a multi-period model.

6.1. Single-Period Optimization Model

Case A and B presented in the previous section are formulated using a single period (i.e., averaging the data for a year). The detailed design is shown in Figure 6. The two cases are elaborated below:

- Case A entails the integration of synthetic methane, SNG, obtained by utilizing CO₂, with conventional NG for distribution in a single-period case. No hydrogen is introduced at the mixing node. The optimal design structure is shown in Figure 4.
- Case B involves integrating synthetic natural gas, SNG, obtained by utilizing CO₂, with hydrogen from electrolysis and conventional natural gas for distribution in a single-period case. The optimal design structure is shown in Figure 7.

Figure 5 shows the detailed discretisation of the time periods. Figure 4 shows the detailed design of the optimized superstructure for the single-period case instance of Case A. Part of the design, indicated by solid blocks in Figure 3, is fixed. The model also includes design decisions to model for the possible expansion of the network, as shown in Figure 4. These are denoted with dashed blocks in the superstructure in Figure 3. The design results show that six power-to-hydrogen sources E1, E4, E6, E7, E8, E9 are developed based on the available electricity generated. The capacity of each of the PtH stations is 10 MW, corresponding to ten configured electrolyzers per PtH unit. For the CO₂ sources, only one source, C2, out of eight possible sources, is developed by the optimization. The CO₂ source is fed into the reaction unit R, shown in Figure 4, before it is combined with the natural gas network. We have three natural gas sources, N1, N2 and N3, already developed in the existing natural gas system, and the optimized design includes two more natural gas sources, N4 and N6. The optimized superstructure also includes a distribution station and one compressor station at node N1. Three blending units M11, M12, and M13 are developed, in addition to eight existing blending units, M1, . . . , M8. Apart from one existing distribution station, D1, two additional distribution nodes, D2 and D3 are included in the design.

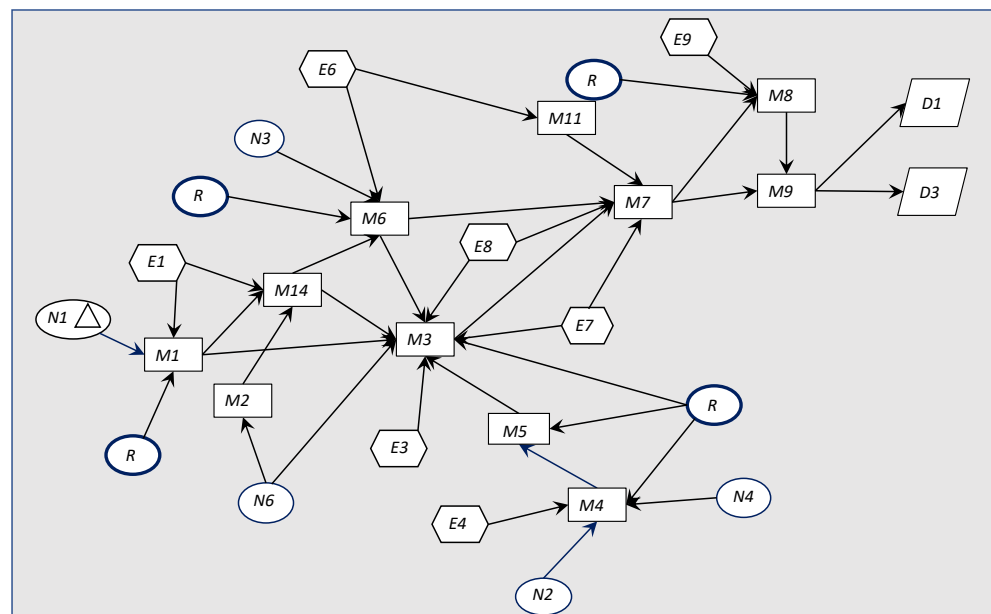


Figure 6. Superstructure for single-period injection of renewables in the Ontario natural gas grid (pipeline distance not to scale).

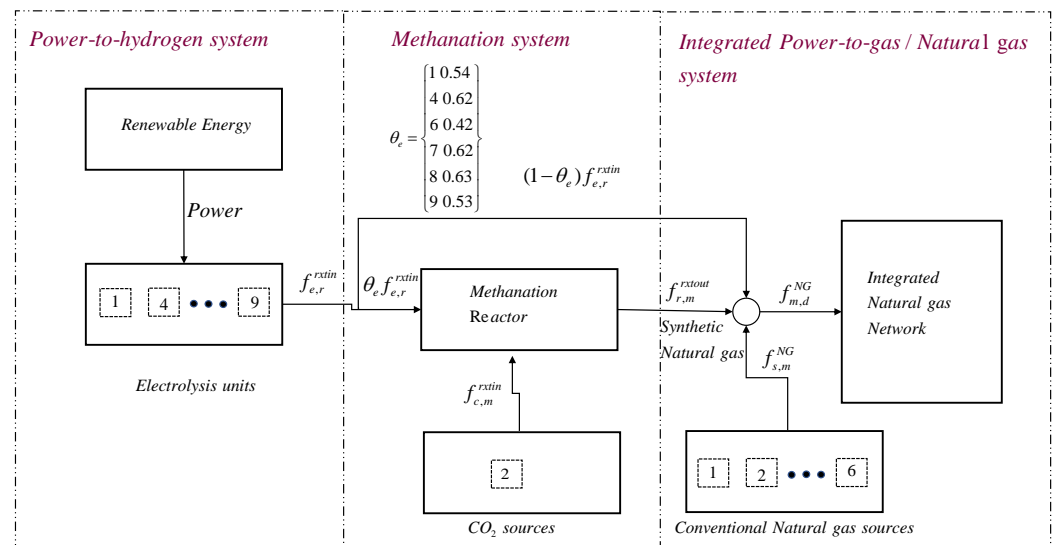


Figure 7. Process description for combined methanation and hydrogen injection into natural gas networks (Case B).

For Case B shown in Figure 7, the same design solution for the three sub-models is obtained: six hydrogen units, one CO₂ source and five natural gas sources are selected in the optimal design. However, for the operational decisions, we find that the optimization recommends a different solution for Case B compared to Case A. The optimizer suggests that partially reacting hydrogen in the reactor, and partially injecting hydrogen directly into the natural gas network in Case B is a better design than Case A, in terms of optimal profit. The values of variable θ , shown in Figure 7, indicate that at some hydrogen nodes, more hydrogen is utilized for methanation than others. The net present value (negative for the optimal objective in Equation (6)) is \$1534.2 M for Case B and \$1522.6 M for Case A. This indicates that the strategy in Case B provides about \$12 M more in revenue. It therefore means that injecting hydrogen directly (i.e., utilizing hydrogen completely for methanation, and the onward injection of methane to the natural gas network) is not the optimal design. The flow rates to the reactor and into the blending nodes are shown on Table 1 for Case A and Table 2 for Case B. In Table 1, the flow rates from the hydrogen stations into the reactor, and then the outlet stream are mixed at the blending points in the natural gas network. On the other hand, Table 2 presents the flow rates in the second design with partial reaction of hydrogen in the reactor. Overall, a greater flow rate into the reactor is realized in Case A because no hydrogen is directly injected into the mixing point in the natural gas network. Although, Case B has a reduced flow of hydrogen into the reactor, it allows partial injection of hydrogen into the natural gas network system. The fraction of hydrogen injected into the natural gas network, denoted by θ_e suggests that on average, more hydrogen is utilized in the reactor for CO₂ consumption.

Table 1. Optimal operation decisions on flow rates for Case A.

Flow Variables To Reactor r			To Blending Unit m	
$f_{e,r}$	$f_{c,r}$	θ_e	$f_{r,m}$	$f_{n,m}$
(E1,R) 130.4	(C2,R) 28	(E1) 1	(R,M1) 31	(N1,M1) 73
(E4,R) 35		(E2) 1	(R,M3) 34	(N2,M4) 876
(E6,R) 31.8		(E3) 1	(R,M4) 36	(N3,M6) 14.3
(E7,R) 81.3		(E4) 1	(R,M5) 35	(N4,M4) 166.4
(E8,R) 25		(E5) 1	(R,M6) 187	(N6,M2) 956
(E9,R) 26		(E5) 1	(R,M8) 33	

Table 2. Optimal operation decisions on flow rates for Case B.

Flow Variables To Reactor r			To Blending Unit m	
$f_{e,r}$	$f_{c,r}$	θ_e	$f_{r,m}$	$f_{n,m}$
(E1,R) 64	(C2,R) 28	(E1) 0.5	(R,M1) 31	(N1,M1) 73
(E4,R) 17		(E4) 0.30	(R,M3) 34	(N2,M4) 876
(E6,R) 19		(E6) 0.56	(R,M4) 36	(N4,M4) 14.3
(E7,R) 23		(E7) 0.19	(R,M5) 35	(N4,M4) 166.4
(E8,R) 25		(E8) 0.65	(R,M6) 33	(N6,M2) 956
(E9,R) 26		(E9) 0.62	(R,M8) 33	

Note: Unit of flow rates is in Mmol/day, where Mmol = 1×10^6 mol. Symbols in bracket are used to denote the indices of the sets, e.g., (E1,R) denotes the connection between nodes E1 and R.

The concentration of hydrogen and CO₂ across the integrated gas network for Case B is shown in Table 3. As shown in Table 1, power-to-gas nodes are developed, giving a total electricity capacity of 60 MW. The optimal cumulative total flow rates across the network are equally shown in Table 3. The single-period case is shown below. Here, the developed pipeline network design, the quality specification for each pipeline connection and the total flow rates are shown. It is evident from Table 3 that the concentration of hydrogen ranges from 0.2 vol % in the pipeline (M3–M14) to 15.1 vol % for the pipeline connecting M6. As for the CO₂ concentration, the optimized design realized lower values compared to the values of hydrogen, ranging from 0.2 to 0.7 vol % across the network. Note that the hydrogen concentration across specific pipelines is zero because no power-to-gas node is developed to supply hydrogen across that source to connection. The maximum hydrogen concentration across the network is 2.5 vol %, within the 5 vol % threshold specified at the distribution centre in nodes D1–D3 in the model. It is worth noting that the model ensures that the concentration of CO₂ meets a very stringent CO₂ emission constraints limit of 1 vol % specified at the exit.

Table 3. Hydrogen and CO₂ concentration (in vol %).

Pipeline Nodes	Hydrogen Conc.	CO ₂ Conc.	Total Flow
Blending units to blending units			
(M1, M14)	3.3	0.7	75
(M2–M14)	-	0.7	955
(M3–M7)	1.7	0.7	2100
(M4–M5)	0.7	0.8	1050
(M5–M3)	0.7	0.8	1050
(M6–M3)	15	0.7	1
(M6–M7)	15	0.7	17
(M7–M8)	2.4	0.7	2138
(M8–M9)	2.5	0.7	2140
(M9–M10)	-	0.2	5725
(M10–M11)	-	0.2	5700
(M14–M3)	0.2	0.7	1030
Blending units to distribution centres			
(M9–D3)	2.5	0.7	2140

6.2. Multi-Period Optimization Model

Here, Case A and B are formulated as a multi-period optimization problem. The number of periods realized for both Case A and B is according to the description in Figure 5. The design for the multi-period case remains the same across the time periods, i.e., problems 2P, 6P, 12P, 18P and 24P have the same design and are shown in Figure 8. However, this design varies from the single-period case. The difference stems from the fact that the connection between blending units M6 and M7 is not optimal in the multi-period formulation, leading the optimization solver to avoid this option.

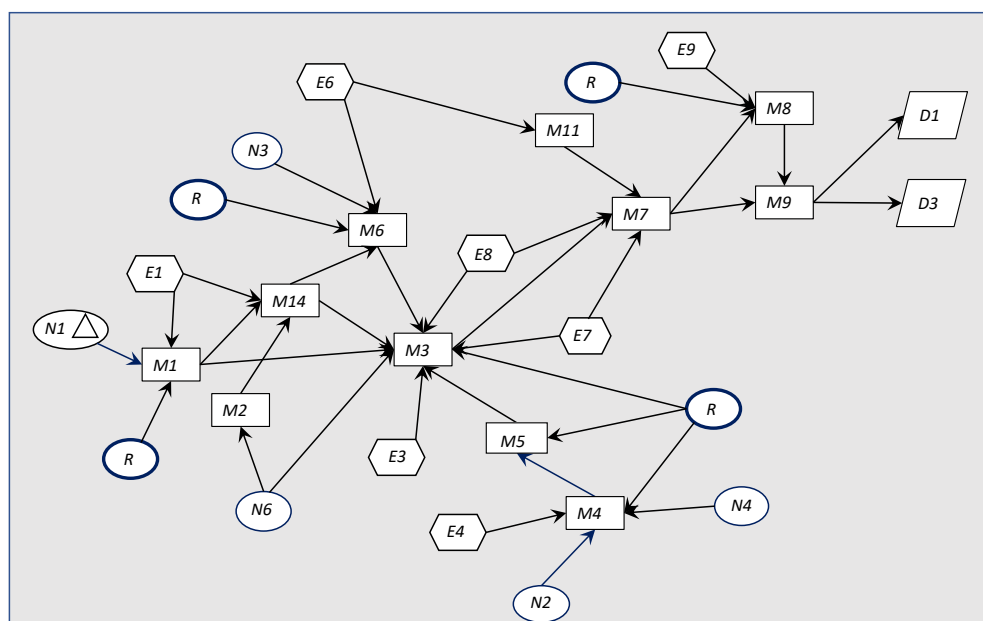


Figure 8. Multi-period design (2P,6P,12P,18P and 24P) of renewable injection into natural gas networks (pipeline distance not to scale).

Tables 4 and 5 present the optimization objective achieved for the different multiperiod settings and the problem size characteristics in terms of model variables and constraints for both Case A and B. As seen from Table 4, the single-period solution (1P case) results in a net present value of \$1522.6 M (obj. val. of −\$1522.6 M), based on the data used. The net present value is obtained with a discount rate of 15% over the considered time period.

Table 4. Multi-period solution summary for Case A (unit for time: seconds).

Problem	1P	2P	6P	12P	18P	24P
ANTIGONE 1.1						
No. of binary var.	113	102	118	122	168	198
No. of cont. var.	1382	879	2758	2297	17,970	26,952
No. of constraints	1552	1552	2932	4471	18,412	27,532
Obj. val. (MM \$)	−1522.6	−1522.6	−1522.5	−1522.4	−1517.8	−1518.9
Relative gap	≤0.1%	≤0.1%	≤0.1%	≤0.1%	≤0.1%	≤0.1%
Total solver time	2	5	11	38	78	143

Table 5. Multi-period solution summary for Case B (unit for time: seconds).

Problem	1P	2P	6P	12P	18P	24P
ANTIGONE 1.1						
No. of binary var.	113	102	138	168	198	228
No. of cont. var.	1382	909	9700	19,384	29,098	33,030
No. of constraints	1552	1595	9460	18,748	28,036	33,292
Obj. val. (MM \$)	−1534.2	−1527.8	−1527.6	−1516.2 [†]	−1511.6 [†]	− [‡]
Relative gap	≤0.1%	≤0.1%	≤0.1%	-	-	-
Total solver time	2	3	13	86,400	86,400	-

Note: A CPU resource limit of 10⁶ is set for the solver, ANTIGONE. [†] Solver was terminated with a feasible solution after a 24 h time limit, without finding the optimal solution. [‡] Solver did not find a feasible solution after 24 h.

Notice that different results are obtained depending on the number of time periods considered in the entire planning horizon of 1 year. This indicates that time averaging of data can affect the solution, and the most conservative solutions are obtained when the data are averaged over shorter time periods, at the expense of more computational burden.

The net present value range for Case A varies from \$1522.6 M for the single-period case to \$1518.9.7 M for the 24P case (i.e., case with 24 periods). Note that as the number of time periods increases, the problem size (number of variables and constraints) also increases. This is important because large problems can pose computational challenges to the optimization solver. For example, Problem 1P and 2P, with one and two periods, respectively, quickly solves and reaches the optimal solution in 2 s. However, the computation time increases significantly when the number of periods increases. The largest problem with 24 periods (24P) requires close to 2 min of solver time to arrive at the optimal solution. As for Case B, the net present value for the 1P and 2P cases was \$1534.2 M and \$1527.8 M, respectively, more than Case A, as discussed in the previous subsection. The solution time for Case B is considerably more than Case A because of the increased number of non-convex terms present in the Case B formulation arising from integrating hydrogen streams into the blending. Problems 1P and 2P reach the optimal solution rapidly; however, cases for 12P and 18P could only attain a feasible solution of \$1516.2 M and \$1311.6 M, respectively, within the allotted time of 24 h. The largest problem with 24 periods (24P) could not find a feasible solution within the time limit of 24 h.

It is evident from the results (and the data used for this study) that Case B, where both hydrogen and synthetic natural gas are partially injected into the integrated network, is an economically more profitable design compared to Case A, where only synthetic natural gas is injected into the natural gas system. This is because the hydrogen pathway provides the needed flexibility required to increase the overall network system revenue. However, as noted from the above discussion, Case B has more computational requirements because of the greater number of non-linear terms (non-convexities) involved. To solve practical case, a small to medium number of time periods should be used.

7. Conclusions and Future Work

The paper presents a novel single- and multi-period optimization model for an integrated system of renewable hydrogen and natural gas (methane) injection across a natural gas network system, using the Ontario natural gas system as a case study. We consider the injection of synthetic methane or SNG with natural gas in Case A, and a combined hydrogen and SNG injection with natural gas in Case B. Furthermore, a multi-period optimization model for the integrated system is developed to account for fluctuations in natural gas demand and electricity generation across different time periods.

The optimal design and operation results suggest that Case B, where both hydrogen and synthetic methane are partially injected into the integrated network, is the best design in terms of better profitability than Case A, where only renewable methane is injected into the natural gas system. The hydrogen-enriched natural gas stream associated with Case B provides extra flexibility for the overall design, leading to more revenue. The superstructure design does not change for the multi-period problem across the different time periods considered in 2P, 6P, 12P, 18P and 24P. There is an increased net present value of approximately \$4 M as the model transitions from a single-period to the 24P multi-period scenario for Case A, while for Case B the 24P case could not be solved within the allotted time limit. The methanation utilization pathway in Case B can aid in upgrading existing biogas plants, which often contain large concentrations of methane, and can substantially increase the renewable content necessary to achieve greenhouse gas reduction targets. However, Case B requires more computational effort to solve.

The integrated model proposed in this paper does not address the separation of hydrogen from natural gas at the end user location. One technology that can achieve the desired separation is called electrochemical hydrogen purification and compression, or EHPC [66]. It works by applying an electrical current across a hydrogen-selective membrane to allow only hydrogen to permeate through it while blocking the natural gas components. Modelling this separation can be a potential future direction. Furthermore, the paper considered profitability as the sole objective in the design and operation of an integrated natural gas system. Future work could consider the detailed environmental impact through a multi-

objective optimization strategy. Note that large time periods (e.g., 24 time periods) could not be solved by ANTIGONE (or other commercial solvers such as BARON [67]) within the time limit. One approach to solve such large-scale multi-period optimization problems for integrated systems is the application duality-based decomposition algorithms [30,59]. These algorithms can efficiently solve large-scale problems primarily because the complex branch and bound search for solving MINLP is performed on small-scale sub-problems, hence substantially improving the solution time for the overall problem. Another approach is to use piece-wise linearization approaches to approximate the non-linear functions [68]. This would consequently reduce the overall computation cost as less expensive surrogates are used to approximate the full model.

Supplementary Materials: The following supporting information can be downloaded at: <https://www.mdpi.com/article/10.3390/en16062631/s1>.

Author Contributions: Conceptualization, E.O., M.F. and A.E.; methodology, E.O.; software, E.O.; validation, E.O., M.F. and A.E.; formal analysis, E.O.; investigation, E.O.; resources, A.E. and A.A.; data curation, E.O.; writing—original draft preparation, E.O.; writing—review and editing, E.O., M.F. and A.E.; visualization, E.O.; supervision, A.E. and M.F.; project administration, A.A.; funding acquisition, A.A., M.F. and A.E. All authors have read and agreed to the published version of the manuscript.

Funding: This work was supported by the Department of Chemical Engineering at the University of Waterloo, Canada Research Chair Tier I—Zero-Emission Vehicles and Hydrogen Energy Systems Grant number: 950-232215, and the Natural Sciences and Engineering Research Council of Canada (NSERC), Discovery Grants Program, RGPIN-2020-04149.

Institutional Review Board Statement: Not applicable.

Informed Consent Statement: Informed consent was obtained from all subjects involved in the study.

Data Availability Statement: The data presented in this study are available on Supplementary Materials.

Conflicts of Interest: The authors declare no conflict of interest.

Abbreviations

The following abbreviations are used in this manuscript:

CO ₂	Carbon dioxide
elec	Electricity
H ₂	Hydrogen
HHV	High heating value
HENG	Hydrogen-enriched natural gas
MILP	Mixed-integer linear program
MINLP	Mixed-integer non-linear program
NG	Natural gas
PEM	Proton exchange membrane
PtH	Power-to-hydrogen
PtG	Power-to-gas
PtM	Power-to-methane
SNG	Synthetic natural gas
rxin	reaction inlet
rxout	reaction outlet

Nomenclature

The list of sets, parameters and variables for the mathematical model are shown in the following table:

Symbols	Description
Sets	
S, E, M, K, T	Source, mixer, distribution station, quality and time horizon sets
S_c, E_c, M_c, Θ_c	Source, mixer, distribution station sets with compressors installed
$\Theta_m, \Theta_d, \Pi_m, \chi_m, \Lambda_m$	Denotes connection from sources to mixers or to distribution centres
E, C, N	Denotes set of electrolyzers, CO ₂ , natural gas, all subset of sources
Parameters	
$\kappa_{n,m}, \kappa_{e,m}, \kappa_{n,d}$	Estimated parameter for pressure–flow profile
α_i	Power consumption parameter at the different nodes i
$p_1, p_2, p_3, conv$	Component coefficients and conversion limit
$c_e^{inv}, c_n^{inv}, c_m^{inv}, c_d^{inv}, c_{n,m}^{inv}, c_{e,m}^{inv}, c_{n,d}^{inv}, c_{m,d}^{inv}$	Coefficient of investment costs
$c_e^{op}, c_n^{op}, c_m^{op}, c_d^{op}, c_{n,m}^{op}, c_{e,m}^{op}, c_{n,d}^{op}, c_n^{elec}$	Coefficient of operating costs
$Z_{e,t}^{lo}, Z_{e,t}^{up}, Z_{c,t}^{lo}, Z_{c,t}^{up}$	Lower and upper bounds on nodal capacity
$F_{e,t}^{lo}, F_{e,t}^{up}$	Lower and upper bounds on electrolyser capacity
$F_{c,t}^{lo}, F_{c,t}^{up}$	Lower and upper bounds on CO ₂ source capacity
$F_{e,t}^{lo}, F_{e,t}^{up}$	Lower and upper bounds on pipeline capacity
$Dem_{d,t}^{lo}, Dem_{d,t}^{up}$	Minimum and maximum demands
U_d, V_d	Quality parameter for natural gas, hydrogen and CO ₂
$W_{i,t}^{lo}, W_{i,t}^{up}$	Lower and upper bounds on the power consumption
$H_2frac_{m,d,t}, CO_2frac_{m,d,t}$	Parameter for hydrogen and CO ₂ fraction
Variables	
Y_e, Y_c, Y_n, Y_m, Y_d	Binary variables for nodes in the system
$Y_{e,r}, Y_{c,r}, Y_{r,m}, Y_{n,m}, Y_{n,d}, Y_{m,m'}, Y_{m,m'}$	Binary variables for connection between nodes or arcs
$f_{e,r,t}, f_{c,r,t}, f_{r,m,t}, f_{n,m,t}, f_{n,d,t}, f_{m,m',w,t}, f_{m,d,w,t}$	Continuous variables denoting flow variables
$s_{m,m',t}, s_{m,d,t}$	Continuous variables denoting flow split fraction
$P_{n,t}^{ups}, P_{m,t}^{ups}, P_{d,t}^{ups}, P_{n,t}^{dws}, P_{m,t}^{dws}, P_{d,t}^{dws}$	Continuous variables denoting upstream and downstream pressures
θ_e	Continuous variable denoting split between hydrogen and natural gas
$E_{(e,t)}, W_{(i,t)}$	Energy required for electrolysis and Power consumption

Appendix A

For some parameter values, e.g., natural gas demand and quality, Problem (1) is slightly infeasible, because of the linking or bridging constraints connecting the three different sub-problem described in the paper. To ensure that the problem is always feasible, the following problem, Problem (A1) is solved instead of Problem (1).

$$\begin{aligned}
& \min_{\substack{y \\ x_1, \dots, x_t, \\ z_1, \dots, z_{n_z}}} \sum_{t=1}^{N_t} [f^0(y) + f_t^1(x_t)] + \sum_{i=1}^{n_z} z_i \\
& \text{s.t. } g^0(y) + g_t^1(x_t) \leq z, \quad \forall t \in \{1, \dots, N_t\}, \\
& \quad x_t \in X_t, \quad \forall t \in \{1, \dots, N_t\}, \\
& \quad y \in \{0, 1\}^{n_y},
\end{aligned} \tag{A1}$$

where z_1, \dots, z_{n_z} are the slack variables needed to ensure feasibility. Notice that the solution of Problem (A1) is only an approximation of the solution of Problem (1).

To achieve the solution for the case study in the paper, we relax the bridging constraints in Equations (21)–(22) as follows:

$$\mathbf{f}_{m,m',k,t} = \mathbf{s}_{m,m'} \left(\sum_{s \in \Theta_{s,m}} \mathbf{f}_{s,m,t} U_{s,k} + \sum_{e \in E_{e,m}} \mathbf{f}_{e,m,t} V_{e,k} + \sum_{r \in R} \mathbf{f}_{r,m,t}^{rxout} + \sum_{m \in \Pi_{m,m'}} \mathbf{f}_{m,m',k,t} \right) + z_1^+ - z_1^-, \tag{A2}$$

$$\mathbf{f}_{m,d,k,t} = \mathbf{s}_{m,d} \left(\sum_{s \in \Theta_{s,m}} \mathbf{f}_{s,m,t} U_{s,k} + \sum_{e \in E_{e,m}} \mathbf{f}_{e,m,t} V_{e,k} + \sum_{r \in R} \mathbf{f}_{r,m,t}^{rxout} + \sum_{m \in \Pi_{m,m'}} \mathbf{f}_{m,m',k,t} \right) + z_2^+ - z_2^-, \tag{A3}$$

$$\sum_{m \in \Pi_{m,m'}} \mathbf{s}_{m,m',t} + \sum_{d \in \Pi_{m,d}} \mathbf{s}_{m,d,t} = 1, \quad \mathbf{s}_{m,m',t}, \mathbf{s}_{m,d,t} \geq 0, \tag{A4}$$

$$\sum_{m \in M} \mathbf{f}_{s,m,t} + \sum_{m \in M} \mathbf{f}_{e,m,t} + \sum_{d \in D} \mathbf{f}_{s,d,t} \leq \mathbf{y}_s Z_{s,t}^{\text{up}} + \mathbf{y}_e Z_{e,t}^{\text{up}} + z_3, \tag{A5}$$

$$\mathbf{f}_{e,t}^{rxin} \leq \theta \mathbf{f}_{e,t}^{H_2} + z_4, \tag{A6}$$

$$\mathbf{f}_{e,m,t} \leq (1 - \theta) \mathbf{f}_{e,t}^{H_2} + z_5, \tag{A7}$$

$$\forall e \in E, \forall m \in M, \forall k \in K, \forall t \in T.$$

where $z_1^+, z_1^-, z_2^+, z_2^-, z_3, z_4, z_5$ are the slack variables.

We can then append the cost of violation of these relaxed constraints to the objective function as follows:

$$\begin{aligned}
\text{objective} &= \text{Capcost} + \sum_{t \in T} \frac{1}{(1+r)^t} (\text{Opcost}_t - \text{Income}_t) \\
&+ z_1^+ + z_1^- + z_2^+ + z_2^- + z_3 + z_4 + z_5.
\end{aligned} \tag{A8}$$

In this case, the following problem is solved:

minimize objective (Equation (A8))

s.t. Integrated hydrogen, methanation and natural gas model in Equations (2)–(20), (23)–(39), (41)–(43), (A2)–(A7),

$\mathbf{y}_n, \mathbf{y}_c, \mathbf{y}_e, \mathbf{y}_m, \mathbf{y}_d, \mathbf{y}_{n,m'}, \mathbf{y}_{e,m'}, \mathbf{y}_{c,m'}, \mathbf{y}_{n,d'}, \mathbf{y}_{m,m'}$, and $\mathbf{y}_{m,d} \in \{0, 1\}$,

All flow rates and pressures are non-negative.

References

1. U.S. Energy-Related Carbon Dioxide Emissions. 2021. Available online: <https://www.eia.gov/environment/emissions/carbon/> (accessed on 23 December 2022).
2. Natural Gas Explained: Natural Gas and the Environment. Available online: <https://www.eia.gov/energyexplained/natural-gas/natural-gas-and-the-environment> (accessed on 23 December 2022).
3. Aruna, C. Investigating the Role of Natural Gas and Hydrogen in a Future Integrated Energy System. Ph.D. Thesis, University College Dublin, Dublin, Ireland, 2022.

4. Maroufmashat, A.; Fowler, M. Transition of Future Energy System Infrastructure; through Power-to-Gas Pathways. *Energies* **2017**, *10*, 1089. [[CrossRef](#)]
5. Sani, S.A.; Maroufmashat, A.; Babonneau, F.; Bahn, O.; Delage, E.; Haurie, A.; Mousseau, N.; Vaillancourt, K. Energy Transition Pathways for Deep Decarbonization of the Greater Montreal Region: An Energy Optimization Framework. *Energies* **2022**, *15*, 3760. [[CrossRef](#)]
6. Rios-Mercado, R.Z.; Borraz-Sánchez, C. Optimization problems in natural gas transportation systems: A state-of-the-art review. *Appl. Energy* **2015**, *147*, 536–555. [[CrossRef](#)]
7. Global Hydrogen Review 2021. Available online: <https://www.iea.org/reports/global-hydrogen-review-2021/executive-summary> (accessed on 27 December 2022).
8. Altfeld, K.; Pinchbeck, D. Admissible hydrogen concentrations in natural gas systems. *Gas Energy* **2013**, *3*, 2013.
9. Collet, P.; Flottes, E.; Favre, A.; Raynal, L.; Pierre, H.; Capela, S.; Peregrina, C. Techno-economic and Life Cycle Assessment of methane production via biogas upgrading and power to gas technology. *Appl. Energy* **2017**, *192*, 282–295. [[CrossRef](#)]
10. Melaina, M.W.; Antonia, O.; Penev, M. *Blending Hydrogen into Natural Gas Pipeline Networks: A Review of Key Issues*; Technical Report; National Renewable Energy Lab. (NREL): Golden, CO, USA, 2013.
11. Mukherjee, U.; Elsholkami, M.; Walker, S.; Fowler, M.; Elkamel, A.; Hajimiragha, A. Optimal sizing of an electrolytic hydrogen production system using an existing natural gas infrastructure. *Int. J. Hydrogen Energy* **2015**, *40*, 9760–9772. [[CrossRef](#)]
12. Schaaf, T.; Grünig, J.; Schuster, M.R.; Rothenfluh, T.; Orth, A. Methanation of CO₂—Storage of Renewable Energy in a Gas Distribution System. *Energy, Sustain. Soc.* **2014**, *4*, 2. [[CrossRef](#)]
13. Schiebahn, S.; Grube, T.; Robinius, M.; Tietze, V.; Kumar, B.; Stolten, D. Power to gas: Technological overview, systems analysis and economic assessment for a case study in Germany. *Int. J. Hydrogen Energy* **2015**, *40*, 4285–4294. [[CrossRef](#)]
14. El Sibai, A.; Rihko-Struckmann, L.; Sundmacher, K. Synthetic methane from CO₂: Dynamic optimization of the Sabatier process for power-to-gas applications. In *Computer Aided Chemical Engineering*; Elsevier: Amsterdam, The Netherlands, 2015; Volume 37, pp. 1157–1162.
15. Üster, H.; Dilaveroglu, Ş. Optimization for design and operation of natural gas transmission networks. *Appl. Energy* **2014**, *133*, 56–69. [[CrossRef](#)]
16. da Silva Alves, F.; de Souza, J.N.M.; Costa, A.L.H. Multi-objective design optimization of natural gas transmission networks. *Comput. Chem. Eng.* **2016**, *93*, 212–220. [[CrossRef](#)]
17. Mikolajková, M.; Haikarainen, C.; Saxén, H.; Pettersson, F. Optimization of a natural gas distribution network with potential future extensions. *Energy* **2017**, *125*, 848–859. [[CrossRef](#)]
18. Ben-Tal, A.; Eiger, G.; Gershovitz, V. Global minimization by reducing the duality gap. *Math. Program.* **1994**, *63*, 193–212. [[CrossRef](#)]
19. Kolodziej, S.P.; Grossmann, I.E.; Furman, K.C.; Sawaya, N.W. A discretization-based approach for the optimization of the multiperiod blend scheduling problem. *Comput. Chem. Eng.* **2013**, *53*, 122–142. [[CrossRef](#)]
20. Bagajewicz, M.; Rodera, H.; Savelski, M. Energy efficient water utilization systems in process plants. *Comput. Chem. Eng.* **2002**, *26*, 59–79. [[CrossRef](#)]
21. Bagajewicz, M. A review of recent design procedures for water networks in refineries and process plants. *Comput. Chem. Eng.* **2000**, *24*, 2093–2113. [[CrossRef](#)]
22. Haverly, C.A. Studies of the behavior of recursion for the pooling problem. *ACM Sigmap Bull.* **1978**, *25*, 19–28. [[CrossRef](#)]
23. Alfaki, M.; Haugland, D. Strong formulations for the pooling problem. *J. Glob. Optim.* **2013**, *56*, 897–916. [[CrossRef](#)]
24. Tawarmalani, M.; Sahinidis, N.V. *Convexification and Global Optimization in Continuous and Mixed-Integer Nonlinear Programming: Theory, Algorithms, Software, and Applications*; Springer Science & Business Media: Berlin/Heidelberg, Germany, 2002; Volume 65.
25. Floudas, C.A. *Deterministic Global Optimization: Theory, Methods and Applications*; Springer Science & Business Media: Berlin/Heidelberg, Germany, 2013; Volume 37.
26. Selot, A.; Kuok, L.K.; Robinson, M.; Mason, T.L.; Barton, P.I. A short-term operational planning model for natural gas production systems. *AIChE J.* **2008**, *54*, 495–515. [[CrossRef](#)]
27. Chiang, N.Y.; Zavala, V.M. Large-scale optimal control of interconnected natural gas and electrical transmission systems. *Appl. Energy* **2016**, *168*, 226–235. [[CrossRef](#)]
28. Correa-Posada, C.M.; Sánchez-Martín, P. Integrated power and natural gas model for energy adequacy in short-term operation. *IEEE Trans. Power Syst.* **2015**, *30*, 3347–3355. [[CrossRef](#)]
29. Ogbe, E.; Mukherjee, U.; Fowler, M.; Almansoori, A.; Elkamel, A. Integrated Design and Operation Optimization of Hydrogen Commingled with Natural Gas in Pipeline Networks. *Ind. Eng. Chem. Res.* **2020**, *59*, 1584–1595. [[CrossRef](#)]
30. Li, X.; Tomasgard, A.; Barton, P.I. Nonconvex generalized Benders decomposition for Stochastic Separable Mixed-Integer Nonlinear Programs. *J. Optim. Theory Appl.* **2011**, *151*, 425–454. [[CrossRef](#)]
31. Clegg, S.; Mancarella, P. Integrated modeling and assessment of the operational impact of power-to-gas (P2G) on electrical and gas transmission networks. *IEEE Trans. Sustain. Energy* **2015**, *6*, 1234–1244. [[CrossRef](#)]
32. de Boer, H.S.; Grond, L.; Moll, H.; Benders, R. The application of power-to-gas, pumped hydro storage and compressed air energy storage in an electricity system at different wind power penetration levels. *Energy* **2014**, *72*, 360–370. [[CrossRef](#)]
33. Nastasi, B.; Basso, G.L. Hydrogen to link heat and electricity in the transition towards future Smart Energy Systems. *Energy* **2016**, *110*, 5–22. [[CrossRef](#)]

34. Sahinidis, N.; Grossmann, I. Reformulation of multiperiod MILP models for planning and scheduling of chemical processes. *Comput. Chem. Eng.* **1991**, *15*, 255–272. [[CrossRef](#)]
35. Ortíz-Gómez, A.; Rico-Ramírez, V.; Hernández-Castro, S. Mixed-integer multiperiod model for the planning of oilfield production. *Comput. Chem. Eng.* **2002**, *26*, 703–714. [[CrossRef](#)]
36. Misener, R.; Floudas, C.A. ANTIGONE: Algorithms for continuous/integer global optimization of nonlinear equations. *J. Glob. Optim.* **2014**, *59*, 503–526. [[CrossRef](#)]
37. Unsihay, C.; Lima, J.M.; De Souza, A.Z. Modeling the integrated natural gas and electricity optimal power flow. In Proceedings of the 2007 IEEE Power Engineering Society General Meeting, Tampa, FL, USA, 24–28 June 2007; pp. 1–7.
38. Qiu, J.; Dong, Z.Y.; Zhao, J.H.; Meng, K.; Zheng, Y.; Hill, D.J. Low carbon oriented expansion planning of integrated gas and power systems. *IEEE Trans. Power Syst.* **2015**, *30*, 1035–1046. [[CrossRef](#)]
39. Liu, C.; Shahidehpour, M.; Wang, J. Application of augmented Lagrangian relaxation to coordinated scheduling of interdependent hydrothermal power and natural gas systems. *IET Gener. Transm. Distrib.* **2010**, *4*, 1314–1325. [[CrossRef](#)]
40. El-Hadary, M.I.; Senthilraja, S.; Zayed, M.E. A hybrid system coupling spiral type solar photovoltaic thermal collector and electrocatalytic hydrogen production cell: Experimental investigation and numerical modeling. *Process Saf. Environ. Prot.* **2023**, *170*, 1101–1120. [[CrossRef](#)]
41. Calero, F.; Cañizares, C.A.; Bhattacharya, K.; Anierobi, C.; Calero, I.; de Souza, M.F.Z.; Farrokhhabadi, M.; Guzman, N.S.; Mendieta, W.; Peralta, D.; et al. A Review of Modeling and Applications of Energy Storage Systems in Power Grids. *Proc. IEEE* **2022**, 1–26. . [[CrossRef](#)]
42. Garmsiri, S.; Rosen, M.A.; Smith, G.R. Integration of wind energy, hydrogen and natural gas pipeline systems to meet community and transportation energy needs: A parametric study. *Sustainability* **2014**, *6*, 2506–2526. [[CrossRef](#)]
43. Guandalini, G.; Colbertaldo, P.; Campanari, S. Dynamic modeling of natural gas quality within transport pipelines in presence of hydrogen injections. *Appl. Energy* **2017**, *185*, 1712–1723. [[CrossRef](#)]
44. Eames, I.; Austin, M.; Wojcik, A. Injection of gaseous hydrogen into a natural gas pipeline. *Int. J. Hydrogen Energy* **2022**, *47*, 25745–25754. [[CrossRef](#)]
45. Su, Y.; Li, J.; Guo, W.; Zhao, Y.; Li, J.; Zhao, J.; Wang, Y. Prediction of Mixing Uniformity of Hydrogen Injection in Natural Gas Pipeline Based on a Deep Learning Model. *Energies* **2022**, *15*, 8694. [[CrossRef](#)]
46. Liu, J.; Teng, L.; Liu, B.; Han, P.; Li, W. Analysis of Hydrogen Gas Injection at Various Compositions in an Existing Natural Gas Pipeline. *Front. Energy Res.* **2021**, *9*, 685079. [[CrossRef](#)]
47. Tong, S.; Li, X.; Sun, S.; Tu, C.; Xia, X. Interchangeability of Hydrogen Injection in Zhejiang Natural Gas Pipelines as a Means to Achieve Carbon Neutrality. *Energies* **2022**, *15*, 6394. [[CrossRef](#)]
48. Ekhtiari, A.; Flynn, D.; Syron, E. Investigation of the Multi-Point Injection of Green Hydrogen from Curtailed Renewable Power into a Gas Network. *Energies* **2020**, *13*, 6047. [[CrossRef](#)]
49. Keogh, N.; Corr, D.; O’Shea, R.; Monaghan, R. The gas grid as a vector for regional decarbonisation—A techno economic case study for biomethane injection and natural gas heavy goods vehicles. *Appl. Energy* **2022**, *323*, 119590. [[CrossRef](#)]
50. El Sibai, A.; Rihko Struckmann, L.K.; Sundmacher, K. Model-based Optimal Sabatier Reactor Design for Power-to-Gas Applications. *Energy Technol.* **2017**, *5*, 911–921. [[CrossRef](#)]
51. Wang, B.; Liang, Y.; Zheng, J.; Qiu, R.; Yuan, M.; Zhang, H. An MILP model for the reformation of natural gas pipeline networks with hydrogen injection. *Int. J. Hydrogen Energy* **2018**, *43*, 16141–16153. [[CrossRef](#)]
52. Wang, J.; Zeng, P.; Li, Y.; Liu, J. Optimal Capacity Planning of Power to Hydrogen in Integrated Electricity–Hydrogen–Gas Energy Systems Considering Flexibility and Hydrogen Injection. *Front. Energy Res.* **2022**, *10*, 845637. [[CrossRef](#)]
53. Li, X.; Armagan, E.; Tomasgard, A.; Barton, P.I. Stochastic pooling problem for natural gas production network design and operation under uncertainty. *AIChE J.* **2011**, *57*, 2120–2135. [[CrossRef](#)]
54. Middleton, R.S.; Bielicki, J.M. A scalable infrastructure model for carbon capture and storage: SimCCS. *Energy Policy* **2009**, *37*, 1052–1060. [[CrossRef](#)]
55. Hasan, M.F.; Boukouvala, F.; First, E.L.; Floudas, C.A. Nationwide, regional, and statewide CO₂ capture, utilization, and sequestration supply chain network optimization. *Ind. Eng. Chem. Res.* **2014**, *53*, 7489–7506. [[CrossRef](#)]
56. Tebibel, H.; Labeled, S. Design and sizing of stand-alone photovoltaic hydrogen system for HCNG production. *Int. J. Hydrogen Energy* **2014**, *39*, 3625–3636. [[CrossRef](#)]
57. Buasri, P. Photovoltaic Array Sizing for PV-Electrolyzer. *World Acad. Sci. Technol. J.* **2010**, *71*, 641–644.
58. Eichman, J.; Harrison, K.; Peters, M. *Novel Electrolyzer Applications: Providing More than Just Hydrogen*; Technical Report; National Renewable Energy Laboratory (NREL): Golden, CO, USA, 2014.
59. Li, D.; Li, X. A new optimization model and a customized solution method for natural gas production network design and operation. *AIChE J.* **2017**, *63*, 933–948. [[CrossRef](#)]
60. Han, J.; Lee, I. Multiperiod stochastic optimization model for carbon capture and storage infrastructure under uncertainty in CO₂ emissions, product prices, and operating costs. *Ind. Eng. Chem. Res.* **2012**, *51*, 11445–11457. [[CrossRef](#)]
61. McCarl, B.A.; Meeraus, A.; van der Eijk, P.; Bussieck, M.; Dirkse, S.; Steacy, P.; Nelissen, F. *McCarl GAMS User Guide*; GAMS Development Corporation: Fairfax, VA, USA, 2004.
62. Drud, A.S. CONOPT—A large-scale GRG code. *ORSA J. Comput.* **1994**, *6*, 207–216. [[CrossRef](#)]

63. IBM ILOG CPLEX. *V12. 1: User's Manual for CPLEX*; International Business Machines Corporation: Armonk, NY, USA, 2009; Volume 46, p. 157.
64. Mitra, S.; Garcia-Herreros, P.; Grossmann, I. A Novel Cross-decomposition Multi-cut Scheme for Two-Stage Stochastic Programming. *Comput. Aided Chem. Eng.* **2014**, *22*, 241–246.
65. Ogbe, E.; Li, X. A new cross decomposition method for stochastic mixed-integer linear programming. *Eur. J. Oper. Res.* **2017**, *256*, 487–499. [[CrossRef](#)]
66. Rhandi, M.; Trégaro, M.; Druart, F.; Deseure, J.; Chatenet, M. Electrochemical hydrogen compression and purification versus competing technologies: Part I. Pros and cons. *Chin. J. Catal.* **2020**, *41*, 756–769. [[CrossRef](#)]
67. Sahinidis, N.V. BARON: A general purpose global optimization software package. *J. Glob. Optim.* **1996**, *8*, 201–205. [[CrossRef](#)]
68. Carneiro, M.; Misener, R.; Floudas, C. Piecewise-Linear Approximations of Multidimensional Functions. *J. Optim. Theory Appl.* **2010**, *145*, 120–147.

Disclaimer/Publisher's Note: The statements, opinions and data contained in all publications are solely those of the individual author(s) and contributor(s) and not of MDPI and/or the editor(s). MDPI and/or the editor(s) disclaim responsibility for any injury to people or property resulting from any ideas, methods, instructions or products referred to in the content.